Diffractions of Flexural Waves by a Cavity in an Elastic Plate

YIH-HSING PAO*
Cornell University, Ithaca, N. Y.
AND
C. C. CHAO†
Stanford University, Stanford, Calif.

Based on Mindlin's theory of flexural motions of plates, which takes into account the rotatory inertia and shear effects, diffractions of flexural waves by a circular inclusion in an elastic plate are investigated. An incident plane flexural wave passing through the inclusion is scattered into three types of flexural waves. From the combined incident and scattered waves, moment and shear on the boundary of the cavity are computed. They are the dynamical moment and shear concentrations in a vibratory plate with a cavity. Moment concentration factors are found to be lower in the dynamic case than in the static case.

I. Introduction

IN this paper we investigate the diffraction of a plane flexural wave by a circular cavity in an elastic plate, based on Mindlin's theory of flexural motions of plates.[1] According to their velocities and modes, waves in a plate in flexure may be divided into three types: slow flexural, fast flexural, and thickness shear waves. Kane[2] has shown that, in general, any one of these waves propagating toward the edge of a semi-infinite plate gives rise to reflected waves of all three types.

When a plane flexural wave passes through an inclusion, be it a cavity, or a rigid or elastic insert, part of the incident wave is scattered into three waves. The source that emits the incident wave may be a force applied perpendicularly to the plate, varying harmonically in time and located at a distance sufficiently far away from the inclusion. The combination of the incident and the three scattered waves constitute the diffracted flexural waves in the plate.

From the wave motion, displacements, moments, and shears everywhere in a plate can be determined. Of particular interest are the moment and shear around a circular cavity in a plate. It is well known that the moment around the cavity is larger than the uniform bending moment applied statically to the plate.[3] Subjected to the same loading, the ratio of the maximum value of moment near the cavity to the average value in the plate without the cavity is called the moment concentration factor. For plain bending, a factor as high as 3 has been shown by Reissner.[4]

If the plate is set into motion by the propagating flexural waves, in this study, moment and shear concentration factors are found to be different from the statical ones. Their magnitudes depend on the Poisson's ratio and thickness of the plate, radius of the cavity, and the wavelength or the frequency of the traveling waves.

For a small cavity in a thick plate, the dynamical moment concentration factor of a plate in flexural motion is the same as the stress concentration factor of a thin plate in extensional motion given in Ref. 5. When the frequency approaches zero, the dynamical factor reduces to the statical one given by Reissner. When frequency increases, the values of moment and shear concentration factors are found to be decreasing.

Presented as Preprint 64-79 at the AIAA Aerospace Sciences Meeting, New York, January 20–22, 1964; revision received June 8, 1964. This investigation was supported by the U. S. Army Research Office (Durham) under Grant No. DA-ORD-31-124-G238.

* Associate Professor, Department of Engineering Mechanics.
† Associate Professor, Department of Aeronautics and Astronautics.

In the next section, we briefly present Mindlin's theory. Incident and scattered waves in general are discussed in Sec. III, and diffraction by a circular cavity is discussed in Sec. IV. Section V presents the dynamical moment and shear concentration factors, followed by a few remarks. The corresponding statical ones are discussed in the Appendix.

II. Mindlin's Theory

In Ref. 1, the displacement components of a plate in steady-state flexural motion, when referred to Cartesian coordinates, are assumed as

$$u_x = z\psi_x(x, y)e^{-ipt} \qquad u_y = z\psi_y(x, y)e^{-ipt}$$
$$u_z = w(x, y)e^{-ipt} \tag{2.1a}$$

where z axis is chosen to be perpendicular to the middle plane of the plate (Fig. 1), and p is the circular frequency. The three plate displacements ψ_x, ψ_y, and w can be expressed in terms of three displacement potentials $\eta_i(x, y)$ as

$$\left.\begin{aligned}\psi_x &= (\sigma_1 - 1)\frac{\partial\eta_1}{\partial x} + (\sigma_2 - 1)\frac{\partial\eta_2}{\partial x} + \frac{\partial\eta_3}{\partial y}\\ \psi_y &= (\sigma_1 - 1)\frac{\partial\eta_1}{\partial y} + (\sigma_2 - 1)\frac{\partial\eta_2}{\partial y} - \frac{\partial\eta_3}{\partial x}\\ w &= \eta_1 + \eta_2\end{aligned}\right\} \tag{2.2a}$$

and each potential satisfies a Helmholtz equation

$$(\nabla^2 + \delta_i^2)\eta_i = 0 \qquad i = 1, 2, 3 \tag{2.3}$$

The potential η_1 generates the slow flexural waves, η_2 the fast flexural, and η_3 the thickness shear waves. In the foregoing equations,

$$\left.\begin{aligned}\delta_{1,2}^2 &= \frac{\pi^2p^2}{24\kappa^2p_0^2}\left\{\frac{1}{S} + \frac{1}{R} \pm \left[\frac{1}{R^2} + \frac{1}{S^2} + \frac{2}{RS}\left(\frac{24\kappa^2p_0^2}{\pi^2p^2} - 1\right)\right]^{1/2}\right\}\\ \delta_3^2 &= \frac{\pi^2}{h^2}\left(\frac{p^2}{p_0^2} - \frac{12\kappa^2}{\pi^2}\right)\\ \sigma_1 &= \frac{2}{1-\nu}\left(\frac{\delta_2}{\delta_3}\right)^2 \qquad \sigma_2 = \frac{2}{1-\nu}\left(\frac{\delta_1}{\delta_3}\right)^2\\ R &= \frac{h^2}{12} \qquad S = \frac{D}{\kappa^2Gh} = \frac{h^2}{6\kappa^2(1-\nu)}\\ D &= \frac{Gh^3}{6(1-\nu)} \qquad p_0 = \frac{\pi c_2}{h}\end{aligned}\right\} \tag{2.4}$$

where h is the thickness of the plate, ν the Poisson's ratio, G the shear modulus, κ^2 the shear coefficient, and c_2 the shear wave velocity in an infinite elastic solid. The p_0 that is chosen to normalize the frequencies is the lowest circular frequency of the simple thickness shear modes of a plate based on the three-dimensional theory. Unless otherwise noted, the shear coefficient κ^2 assumes the value[1] $\pi^2/12$, so that the cut-off frequency of the second mode of Mindlin's theory is identical with p_0.

The three wave numbers δ_i are dependent on the frequencies; thus, all three flexural waves are dispersive. Furthermore, δ_1 is real for all frequencies, whereas δ_2 and δ_3 may be real or imaginary according to whether $p > p_0$ or $p < p_0$. Imaginary wave numbers correspond to attenuating modes with an exponentially decaying factor in space coordinates. Variations of the normalized wave numbers $\delta_i h$ vs p/p_0 are shown in Fig. 2.

If $p = p_0$, we have a degenerate case because of the vanishing δ_2 and δ_3. This case can be better analyzed with another set of displacement potentials and equations discussed in Ref. 6.

The moments M and shears Q are related to the plate displacements as

$$\left.\begin{aligned} M_x &= D\left(\frac{\partial\psi_x}{\partial x} + \nu\frac{\partial\psi_y}{\partial y}\right) \\ M_y &= D\left(\frac{\partial\psi_y}{\partial y} + \nu\frac{\partial\psi_x}{\partial x}\right) \\ M_{yx} &= \frac{1-\nu}{2}D\left(\frac{\partial\psi_x}{\partial y} + \frac{\partial\psi_y}{\partial x}\right) \\ Q_x &= \kappa^2 Gh\left(\frac{\partial w}{\partial x} + \psi_x\right) \\ Q_y &= \kappa^2 Gh\left(\frac{\partial w}{\partial y} + \psi_y\right) \end{aligned}\right\} \qquad (2.5a)$$

In terms of cylindrical coordinates (r, θ, z), Eqs. (1a, 2a, and 5a) take, respectively, the following forms:

$$\left.\begin{aligned} u_r &= z\psi_r(r,\theta)e^{-ipt} \\ u_\theta &= z\psi_\theta(r,\theta)e^{-ipt} \\ u_z &= w(r,\theta)e^{-ipt} \end{aligned}\right\} \qquad (2.1b)$$

$$\left.\begin{aligned} \psi_r &= (\sigma_1 - 1)\partial\eta_1/\partial r + (\sigma_2 - 1)\partial\eta_2/\partial r + r^{-1}\partial\eta_3/\partial\theta \\ \psi_\theta &= (\sigma_1 - 1)r^{-1}\partial\eta_1/\partial\theta + \\ &\qquad (\sigma_2 - 1)r^{-1}\partial\eta_2/\partial\theta - \partial\eta_3/\partial r \\ w &= \eta_1 + \eta_2 \end{aligned}\right\} \qquad (2.2b)$$

$$\left.\begin{aligned} M_r &= D[\partial\psi_r/\partial r + \nu r^{-1}(\psi_r + \partial\psi_\theta/\partial\theta)] \\ M_\theta &= D[r^{-1}(\partial\psi_\theta/\partial\theta + \psi_r) + \nu\partial\psi_r/\partial r] \\ M_{r\theta} &= \tfrac{1}{2}(1-\nu)D[r^{-1}(\partial\psi_r/\partial\theta - \psi_\theta) + \partial\psi_\theta/\partial r] \\ Q_r &= \kappa^2 Gh(\psi_r + \partial w/\partial r) \\ Q_\theta &= \kappa^2 Gh(\psi_\theta + r^{-1}\partial w/\partial\theta) \end{aligned}\right\} \qquad (2.5b)$$

Equations (2.1–2.5) constitute a complete set of equations of flexural motions of plates. The boundary conditions for the plate are usually prescribed in terms of displacements, moments, and shears. A unique solution is assured if, on the edge of the plate, any combination that contains one member of each of the following three pairs is known:

$$\psi_n M_n \qquad \psi_s M_{ns} \qquad wQ_n \qquad (2.6)$$

where the n and s indicate, respectively, the normal and tangential directions to the edge.

If the effect of shear and rotatory inertia are neglected, the foregoing equations reduce to those of classical plate theory. The transition is done by setting R and S in (2.4) equal to zero.

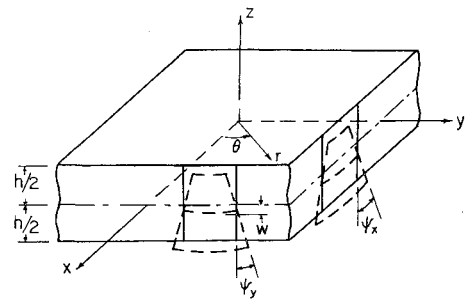

Fig. 1 Plate geometry and plate displacements.

III. Incident and Scattered Waves

The three types of flexural waves, the slow flexural, the fast flexural, and thickness shear may propagate independently in an infinite plate. They are, however, coupled in a plate with rigid or traction free edges since none of them alone can meet the boundary conditions. This is shown in Ref. 2 for the reflection of waves at the edge of a plate and in numerous investigations of flexural vibrations of plates such as in Ref. 7. In this and the next sections, we shall show that the scattering of an incident wave by an inclusion in a plate is also comprised of all three types of waves. Only incident slow flexural waves will be considered here.

A slow flexural wave, propagating in the positive x direction (Fig. 1), can be represented mathematically by

$$\eta_1^{(i)} = \eta_0 \exp i(\delta_1 x - pt) \qquad \eta_2^{(i)} = \eta_3^{(i)} = 0 \qquad (3.1a)$$

The corresponding plate displacements, moments, and shears with the exponential function $\exp i(\delta_1 x - pt)$ omitted are

$$\psi_x = i\delta_1(\sigma_1 - 1)\eta_0 \qquad \psi_y = 0 \qquad w = \eta_0 \qquad (3.2a)$$

$$\begin{aligned} M_x &= M_0 \qquad M_y = \nu M_0 \\ Q_x &= iQ_0 \qquad M_{xy} = Q_y = 0 \end{aligned} \qquad (3.3a)$$

where

$$M_0 = -D\delta_1^2(\sigma_1 - 1)\eta_0 \qquad Q_0 = \kappa^2 Gh\delta_1\sigma_1\eta_0 \qquad (3.4)$$

are the maximum bending moment and shear, respectively, in the plate. Both M_0 and Q_0 are frequency dependent As p/p_0 approaches zero, M_0 vanishes in the order of $(p/p_0)^2$, whereas Q_0 vanishes in the order of $(p/p_0)^3$. In the limit, by letting η_0 be infinity, such that

$$M_0' = D\delta_1^2\eta_0 \qquad (3.4a)$$

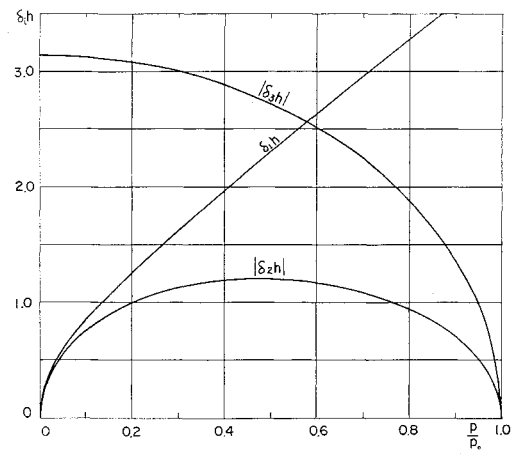

Fig. 2 Normalized wave numbers $\delta_i h$ vs normalized frequencies p/p_0.

is finite, the shear at zero frequency vanishes, and the plate is subjected to moments M_0' and $\nu M_0'$ at two perpendicular directions. We shall designate the flexural motion described by Eqs. (3.1–3.3) as the undisturbed state. It is the dynamical counterpart of "pure bending" of a plate without an inclusion.

For the convenience of satisfying boundary conditions prescribed over the edge of a cylindrical inclusion centered at the origin, the incident waves and the corresponding displacements, etc. are expressed in polar coordinates by expanding $\exp(i\delta_1 x)$ into a Fourier-Bessel series.[8] The results are

$$\left.\begin{aligned} \eta_1^{(i)} &= \eta_0 \Sigma \epsilon_n i^n J_n(\delta_1 r)\cos n\theta \\ \eta_2^{(i)} &= \eta_3^{(i)} = 0 \\ \epsilon_n &= \begin{cases} 1 & n = 0 \\ 2 & n > 0 \end{cases} \end{aligned}\right\} \tag{3.1b}$$

$$\left.\begin{aligned} \psi_r^{(i)} &= r^{-1}\Sigma\eta_0(\sigma_1 - 1)\,\epsilon_n i^n \delta_1 r J_n'(\delta_1 r)\cos n\theta \\ \psi_\theta^{(i)} &= r^{-1}\Sigma\eta_0(1 - \sigma_1)\,\epsilon_n i^n\, n J_n(\delta_1 r)\sin n\theta \\ w^{(i)} &= \Sigma\eta_0\epsilon_n i^n J_n(\delta_1 r)\cos n\theta \end{aligned}\right\} \tag{3.2b}$$

$$\left.\begin{aligned} M_r^{(i)} &= D(1 - \nu)r^{-2}\Sigma\eta_0(\sigma_1 - 1)\epsilon_n i^n D_{1r}\cos n\theta \\ M_\theta^{(i)} &= D(\nu - 1)r^{-2}\Sigma\eta_0(\sigma_1 - 1)\epsilon_n i^n J_{1r}\cos n\theta \\ M_{r\theta}^{(i)} &= D(1 - \nu)r^{-2}\Sigma\eta_0(\sigma_1 - 1)\epsilon_n i^n E_{1r}\sin n\theta \\ Q_r^{(i)} &= \kappa^2 Ghr^{-1}\Sigma\eta_0\sigma_1\epsilon_n i^n F_{1r}\cos n\theta \\ Q_\theta^{(i)} &= -\kappa^2 Ghr^{-1}\Sigma\eta_0\sigma_1\epsilon_n i^n H_{1r}\sin n\theta \end{aligned}\right\} \tag{3.3b}$$

where all summations in the foregoing equations and in the sequal are over integral n from zero to infinity, and D_{1r}, etc., are given in (3.8). The time factor $\exp(-ipt)$ is omitted in the foregoing equations and hereafter when its existence is apparent.

Scattered waves may be constructed mathematically from the solutions of the wave equations (2.3). Since only waves radiated outward from the inclusion are considered, we have

$$\begin{aligned} \eta_1^{(s)} &= \Sigma A_n H_n(\delta_1 r)\cos n\theta \\ \eta_2^{(s)} &= \Sigma B_n H_n(\delta_2 r)\cos n\theta \\ \eta_3^{(s)} &= \Sigma C_n H_n(\delta_3 r)\sin n\theta \end{aligned} \tag{3.5}$$

where A_n, B_n, and C_n are constants to be determined from the boundary conditions, and

$$H_n(z) = J_n(z) + iY_n(z)$$

is the Hankel function of the first kind with the conventional superscript (1) being omitted. Substitution of (3.5) into (2.2b) and (2.5b) gives rise to the plate displacements and moments corresponding to the scattered waves:

$$\left.\begin{aligned} \psi_r^{(s)} &= r^{-1}\Sigma[A_n(\sigma_1 - 1)\mathfrak{F}_{1r} + B_n(\sigma_2 - 1)\mathfrak{F}_{2r} + C_n\mathfrak{K}_{3r}]\cos n\theta \\ \psi_\theta^{(s)} &= r^{-1}\Sigma[A_n(1 - \sigma_1)\mathfrak{K}_{1r} + B_n(1 - \sigma_2)\mathfrak{K}_{2r} - C_n\mathfrak{F}_{3r}]\sin n\theta \\ w^{(s)} &= \Sigma n^{-1}[A_n\mathfrak{K}_{1r} + B_n\mathfrak{K}_{2r}]\cos n\theta \end{aligned}\right\} \tag{3.6}$$

$$\left.\begin{aligned} M_r^{(s)} &= (1 - \nu)Dr^{-2}\Sigma[A_n(\sigma_1 - 1)\mathfrak{D}_{1r} + B_n(\sigma_2 - 1)\mathfrak{D}_{2r} - C_n\mathcal{E}_{3r}]\cos n\theta \\ M_\theta^{(s)} &= (\nu - 1)Dr^{-2}\Sigma[A_n(\sigma_1 - 1)\mathcal{J}_{1r} + B_n(\sigma_2 - 1)\mathcal{J}_{2r} - C_n\mathcal{E}_{3r}]\cos n\theta \\ M_{r\theta}^{(s)} &= (1 - \nu)Dr^{-2}\Sigma[A_n(\sigma_1 - 1)\mathcal{E}_{1r} + B_n(\sigma_2 - 1)\mathcal{E}_{2r} - C_n\mathcal{G}_{3r}]\sin n\theta \\ Q_r^{(s)} &= \kappa^2 Ghr^{-1}\Sigma[A_n\sigma_1\mathfrak{F}_{1r} + B_n\sigma_2\mathfrak{F}_{2r} + C_n\mathfrak{K}_{3r}]\cos n\theta \\ Q_\theta^{(s)} &= -\kappa^2 Ghr^{-1}\Sigma[A_n\sigma_1\mathfrak{K}_{1r} + B_n\sigma_2\mathfrak{K}_{2r} + C_n\mathfrak{F}_{3r}]\sin n\theta \end{aligned}\right\} \tag{3.7}$$

where, with $(i = 1, 2, 3)$,

$$\left.\begin{aligned} \mathfrak{D}_{ir} &= \{n^2 + n - [\delta_i^2 r^2/(1 - \nu)]\}H_n(\delta_i r) - \delta_i r H_{n-1}(\delta_i r) \\ \mathcal{E}_{ir} &= n(n + 1)H_n(\delta_i r) - n\delta_i r H_{n-1}(\delta_i r) \\ \mathfrak{F}_{ir} &= -nH_n(\delta_i r) + \delta_i r H_{n-1}(\delta_i r) \\ \mathcal{G}_{3r} &= (n^2 + n - \delta_3^2 r^2/2)H_n(\delta_3 r) - \delta_3 r H_{n-1}(\delta_3 r) \\ \mathfrak{K}_{ir} &= nH_n(\delta_i r) \\ \mathcal{J}_{ir} &= \{n^2 + n + \nu[\delta_i^2 r^2/(1 - \nu)]\}H_n(\delta_i r) - \delta_i r H_{n-1}(\delta_i r) \end{aligned}\right\} \tag{3.8}$$

and $D_{ir} = Re[\mathfrak{D}_{ir}]$, . . . , $J_{ir} = Re[\mathcal{J}_{ir}]$, and Re means "rea part of."

IV. Diffracted Waves in Plate with a Cavity

The waves in the plate as diffracted by a circular cavity of radius $r = a$ are determined by superposing the incident and scattered waves:

$$\begin{aligned} \eta_1 &= \eta_1^{(i)} + \eta_1^{(s)} = \Sigma[\eta_0\epsilon_n i^n J_n(\delta_1 r) + A_n H_n(\delta_1 r)]\cos n\theta \\ \eta_2 &= \eta_2^{(i)} + \eta_2^{(s)} = \Sigma B_n H_n(\delta_2 r)\cos n\theta \\ \eta_3 &= \eta_3^{(i)} + \eta_3^{(s)} = \Sigma C_n H_n(\delta_3 r)\sin n\theta \end{aligned} \tag{4.1}$$

Corresponding plate displacements, moments, and shears are also obtained by adding the incident and scattered parts, e.g.,

$$M_r = M_r^{(i)} + M_r^{(s)}, \text{ etc.} \tag{4.2}$$

For a traction free cavity, the coefficients A_n, B_n, and C_n are fixed by the conditions

$$M_r = M_{r\theta} = Q_r = 0 \qquad \text{at} \qquad r = a \tag{4.3}$$

Since the left-hand side of each equation of (4.3) is a complete orthogonal series, each term of the series must also be zero. Thus, conditions (4.3) give rise to three simultaneous algebraic equations sufficiently to determine the three unknown quantities A_n, B_n, and C_n. Substitution of these quantities into (4.1) or (4.2) completes the solution. The final results for M_θ and Q_θ are given below:

$$\begin{aligned} M_\theta &= -\eta_0 D(1 - \nu)r^{-2}\Sigma\epsilon_n i^n(\Delta_{\theta 6}/\Delta)\cos n\theta \\ Q_\theta &= -\eta_0\kappa^2 Ghr^{-1}\Sigma\epsilon_n i^n(\Delta_\theta/\Delta)\sin n\theta \end{aligned} \tag{4.4}$$

with

$$\Delta_{\theta 6} = \begin{vmatrix} (\sigma_1 - 1)J_{1r} & (\sigma_1 - 1)\mathcal{J}_{1r} & (\sigma_2 - 1)\mathcal{J}_{2r} & -\mathcal{E}_{3r} \\ (\sigma_1 - 1)D_{1a} & (\sigma_1 - 1)\mathfrak{D}_{1a} & (\sigma_2 - 1)\mathfrak{D}_{2a} & -\mathcal{E}_{3a} \\ (\sigma_1 - 1)E_{1a} & (\sigma_1 - 1)\mathcal{E}_{1a} & (\sigma_2 - 1)\mathcal{E}_{2a} & -\mathcal{G}_{3a} \\ \sigma_1 F_{1a} & \sigma_1\mathfrak{F}_{1a} & \sigma_2\mathfrak{F}_{2a} & \mathfrak{K}_{3a} \end{vmatrix}$$

$$\Delta_\theta = \begin{vmatrix} \sigma_1 H_{1r} & \sigma_1\mathfrak{K}_{1r} & \sigma_2\mathfrak{K}_{2r} & \mathfrak{F}_{3r} \\ (\sigma_1 - 1)D_{1a} & (\sigma_1 - 1)\mathfrak{D}_{1a} & (\sigma_2 - 1)\mathfrak{D}_{2a} & -\mathcal{E}_{3a} \\ (\sigma_1 - 1)E_{1a} & (\sigma_1 - 1)\mathcal{E}_{1a} & (\sigma_2 - 1)\mathcal{E}_{2a} & -\mathcal{G}_{3a} \\ \sigma_1 F_{1a} & \sigma_1\mathfrak{F}_{1a} & \sigma_2\mathfrak{F}_{2a} & \mathfrak{K}_{3a} \end{vmatrix} \tag{4.5}$$

$$\Delta = \begin{vmatrix} (\sigma_1 - 1)\mathfrak{D}_{1a} & (\sigma_2 - 1)\mathfrak{D}_{2a} & -\mathcal{E}_{3a} \\ (\sigma_1 - 1)\mathcal{E}_{1a} & (\sigma_2 - 1)\mathcal{E}_{2a} & -\mathcal{G}_{3a} \\ \sigma_1\mathfrak{F}_{1a} & \sigma_2\mathfrak{F}_{2a} & \mathfrak{K}_{3a} \end{vmatrix}$$

where $\mathfrak{F}_{2a} = (\mathfrak{F}_{2r})_{r=a}$, etc. Only the first rows of the first two determinants in (4.5) contain variable r.

For a plate with known material property (G, ν, and c_2), given thickness h, and radius of cavity a, Eqs. (4.4) can be used to calculate the moment and shear at any point (r, θ)

of the plate excited by the incident flexural wave. Since the frequency spectra computed from Mindlin's theory are in excellent agreement with those obtained from the three-dimensional theory for frequencies ranging from zero to a value slightly higher than p_0,[9] the foregoing results are expected to be valid also over such a wide frequency range.‡ However, at $p = p_0$, the foregoing results degenerate, and correct values can only be obtained by a tedious limiting process or by using equations given in Ref. 6. Thus, (4.4) should be used only for the cases $p < p_0$ and $p > p_0$. Two limiting cases, thick plate and thin plate, are to be noted.

1. Thick Plate and Small Cavity

If the thickness of the plate is very large in comparison with the radius of the cavity, a simple result can be obtained by taking the limit $a/h \to 0$.

In (2.4), neglecting p_0/p in the radical for large h, we have

$$(\delta_{1,2}a)^2 \to \frac{p^2a^2}{24\kappa^2c_2^2}\left[\frac{h^2}{S}+\frac{h^2}{R} \pm \left(\frac{h^2}{S}-\frac{h^2}{R}\right)\right]$$

Thus,

$$\left.\begin{aligned} &\delta_1 a \to \left(\frac{1-\nu}{2}\right)^{1/2}\frac{pa}{c_2} \\ &\delta_2 a \to pa/\kappa c_2 \qquad \delta_3 a \to pa/c_2 \\ &\sigma_1 \to 2/\kappa^2(1-\nu) \qquad \sigma_2 \to 1 \end{aligned}\right\} \tag{4.6}$$

Substituting these values into (4.4), we find

$$\frac{M_\theta}{M_0} = \frac{1-\nu}{\delta_1{}^2\gamma^2}\,\Sigma\epsilon_n i^n \frac{\Delta'_{\theta\theta}}{\Delta'}\cos n\theta \tag{4.7}$$

where

$$\Delta_{\theta\theta}{}' = \begin{vmatrix} J_{1r} & \mathcal{J}_{1r} & -\mathcal{E}_{3r} \\ D_{1a} & \mathfrak{D}_{1a} & -\mathcal{E}_{3a} \\ E_{1a} & \mathcal{E}_{1a} & -\mathcal{G}_{3a} \end{vmatrix} \qquad \Delta = \begin{vmatrix} \mathfrak{D}_{1a} & -\mathcal{E}_{3a} \\ \mathcal{E}_{1a} & -\mathcal{G}_{3a} \end{vmatrix}$$

and M_0 was defined in (3.4).

Equation (4.7) yields the moment concentration factor in a thick plate with a small cavity. Since the moment and shear are related to stresses $\tau_{\theta\theta}$ and $\tau_{\theta z}$ as

$$M_\theta = \int_{-h/2}^{h/2} \tau_{\theta\theta} z\,dz \qquad Q_\theta = \int_{-h/2}^{h/2} \tau_{\theta z}\,dz$$

M_θ/M_0 may also be regarded as a stress concentration factor. A comparison of (4.7) with the dynamical stress concentration factor§ of a thin plate with a circular cavity in compression shows that they are equal if κ^2 is taken to be unity. The δ_1 then corresponds to the wave number of compressional waves in a thin plate (plane stress); δ_2 ($= \delta_3$) is equivalent to that of shear wave, and σ_1 is the ratio of the velocities of these two waves in thin plate that was designated by k^2 in Ref. 5. When κ^2 takes the value of $\pi^2/12$, there will be a small difference between these two cases.

The same results are observed when comparing the bending moment M_r and twisting moment $M_{r\theta}$ with radial stress τ_{rr} and shearing stress $\tau_{r\theta}$ in plane stress, respectively. We thus conclude that, in the limit of a small cavity in a thick plate, the values of dynamical stress concentration factors in flexure are equal to the corresponding ones in plane stress. The statical counterpart was pointed out in Ref. 4.

‡ For instance, for a steel plate of $\frac{1}{8}$-in. thickness, $p_0 \approx 3$ Mc/sec.

§ Equation (16a) of Ref. 5, when all stresses are normalized by $(-k^2\mu\alpha\phi_0)$.

2. Thin Plate and Large Cavity

In the limit $a/h \to \infty$, the p_0/p term, when multiplied by a^2, in the radical of (2.4) is dominant. Hence,

$$\left.\begin{aligned} (\delta_{1,2}a)^2 &\to \pm\,(6-6\nu)^{1/2}\frac{pa}{c_2}\left(\frac{a}{h}\right) = \pm pa^2\left(\frac{\rho h}{D}\right)^{1/2} \\ \delta_3{}^2a^2 &\to -\,12\kappa^2a^2/h^2 \\ \sigma_{1,2} &\to \pm\,\frac{pa}{(6-6\nu)^{1/2}\kappa^2c_2}\left(\frac{h}{a}\right) \to 0 \end{aligned}\right\} \tag{4.8}$$

The same limiting values are obtained if $R = S = 0$. Physically, the limit of large a/h may be regarded as a large hole in a thin plate, and vanishing R and S imply the omission of the effects of rotatory inertia and shear. In either implication, it seems that the limiting values of the moments of the present investigation should reduce to those of classical plate theory. In fact, p/δ_1 is the same as the phase velocity of flexural waves of classical theory.[10]

But a preliminary study reveals that the limiting values of the present case do not agree with those of classical theory. Details will be given in another report. An analogous case exists in the studying of flexural vibration of circular plate, where, in the limit of thin plate, the frequency equation based on Mindlin's theory[7] does not agree with that of classical theory.

V. Moment and Shear around Cavity

The only nonvanishing moment and shear at the boundary of the cavity are M_θ and Q_θ. Their values are obtained by setting $r = a$ in (4.4). In the following, we shall normalize the moment by M_0 and the shear by Q_0 and use a bar to indicate a normalized quantity at the boundary, e.g.,

$$\bar{M}_\theta \equiv (M_\theta/M_0)_{r=a} \qquad \bar{\theta}_\theta \equiv (Q_\theta/Q_0)_{r=a} \tag{5.1}$$

With $r = a$, the final forms of $\bar{M}_\theta$ and $\bar{Q}_\theta$ used for subsequent calculations are

$$\left.\begin{aligned} \bar{M}_\theta &= (1-\nu)\Sigma\epsilon_n i^n S_n \cos n\theta \\ Q_\theta &= -\Sigma\epsilon_n i^n T_n \sin n\theta \end{aligned}\right\} \tag{5.2}$$

where

$$\left.\begin{aligned} S_n &= [(2i/\pi)(1+\nu)(\sigma_2-\sigma_1)/(1-\nu)\Delta]\times \\ &\quad [(n^4-n^2)/\sigma_2 + \delta_3{}^2a^2(n^2\sigma_1+n-n^2\sigma_1/\sigma_2)/2 + \\ &\quad (n-n^3)\,\mathcal{K}_n(\delta_3a) + (n-n^3-\delta_3{}^2a^2/2)\,\mathcal{K}_n(\delta_2a) + \\ &\quad (n^2-1)\,\mathcal{K}_n(\delta_3a)\,\mathcal{K}_n(\delta_2a)]H_n(\delta_2a)H_n(\delta_3a) \\ T_n &= [(2i/\pi)(\sigma_2-\sigma_1)n/(\sigma_1\delta_1a\Delta)]H_n(\delta_2a)H_n(\delta_3a)\times \\ &\quad \{\sigma_1(n^2+n)\delta_3{}^2a^2 + \sigma_1(\sigma_2\sigma_1-\sigma_2-\sigma_1)(\delta_3a)^4/4 + \\ &\quad [-n^3+n-(n\sigma_2\sigma_1-n\sigma_2+\sigma_1)\delta_3{}^2a^2/2][\mathcal{K}_n(\delta_3a)+ \\ &\quad \mathcal{K}_n(\delta_2a)] + [n^2-1+(\sigma_2\sigma_1-\sigma_2)\delta_3{}^2a^2/2]\times \\ &\quad \mathcal{K}_n(\delta_3a)\,\mathcal{K}_n(\delta_2a)\} \end{aligned}\right\} \tag{5.3}$$

Δ is given in (4.5), and

$$\mathcal{K}_n(z) = zH_{n-1}(z)/H_n(z) \tag{5.4}$$

is the quotient of Hankel functions which has been studied and tabulated by Onoe.[11] Hankel functions with argument δ_1a are eliminated from the expansions of the determinants $\Delta_{\theta\theta}$ and Δ_θ by applying the Wronskian relation[12]

$$J_n(z)H_{n-1}(z) - H_n(z)J_{n-1}(z) = 2i/\pi z$$

Within the range $0 \le p/p_0 < 1$, $\delta_2{}^2$ and $\delta_3{}^2$ in (2.4) are always negative. Note that Hankel functions with imaginary argument iy can be converted to the modified Bessel functions of the second kind with real argument y by the formula[12]

$$H_n{}^{(1)}(iy) = (2/\pi)i^{-n-1}K_n(y) \tag{5.5}$$

and, consequently,

$$\mathcal{K}_n(iy) = -yK_{n-1}(y)/K_n(y) \tag{5.4a}$$

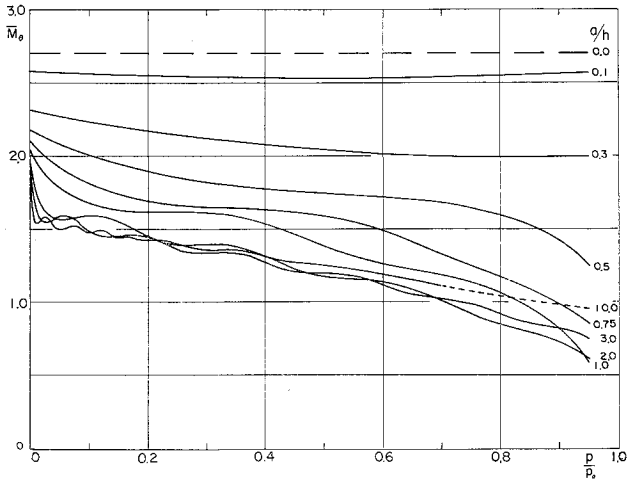

Fig. 3 Absolute values of normalized bending moment $\bar{M}_\theta$ at $r = a$, $\theta = \pi/2$ ($\nu = 0.30$).

After the substitution of (5.4a) into (5.3), only modified Bessel functions with arguments $[\delta_{2,3}a]$ and Hankel functions with argument $\delta_1 a$ (in the denominator) remain.

Values of $\bar{M}_\theta$ and $\bar{Q}_\theta$ will be evaluated for two cases, $p/p_0 \to 0$ and $p/p_0 < 1$, separately. The former should be in agreement with the statical solution, and the latter will reveal the dynamic effect on the amplification of moment and shear.

1. Low Frequency Limit ($p/p_0 \to 0$)

From (2.4), it is clear that, as $p/p_0 \to 0$,

$$\left.\begin{aligned} &\delta_1 a = o(\epsilon) \to 0 \qquad \delta_2 a = o(\epsilon) \to 0 \\ &\qquad \delta_3 a \to i(12)^{1/2}\kappa a/h \end{aligned}\right\}$$
$$\left.\begin{aligned} &\sigma_1 \to o(\epsilon^2) \to 0 \qquad \sigma_2 \to o(\epsilon^2) \to 0 \\ &\qquad \sigma_2/\sigma_1 \to -1 \end{aligned}\right\} \tag{5.6}$$

where $o(\epsilon)$ means "order of infinitesimal ϵ." We thus can approximate the Hankel functions in (5.2) with small arguments $\delta_1 a$ and $\delta_2 a$ by the formulas

$$\left.\begin{aligned} &H_0(z) \to i(2/\pi)\ \ln z \\ &H_n(z) \to -i(n-1)!(2/z)^n/\pi \end{aligned}\right\} \quad \text{as } |z| \to 0 \tag{5.7}$$

The approximate values of S_n and T_n in (5.3) as $p/p_0 \to 0$ are given below:

$$\left.\begin{aligned} &S_0 \to (1+\nu)/(1-\nu) \\ &S_1 \to (1+\nu)\delta_2 a/2(1-\nu) \to 0 \\ &S_n \to \frac{(1+\nu)H_n(\delta_3 a)}{(1+\nu)H_n(\delta_3 a) - 2H_{n-2}(\delta_3 a)} \cdot \frac{(\delta_1 a/2)^{n-2}}{(n-2)!} \\ &\quad \to \begin{cases} \dfrac{(1+\nu)H_2(\delta_3 a)}{(1+\nu)H_2(\delta_3 a) - 2H_0(\delta_3 a)} & n = 2 \\ 0 & n > 2 \end{cases} \end{aligned}\right\} \tag{5.8a}$$

$$\left.\begin{aligned} &T_1 \to \frac{2H_1(\delta_3 a) - \delta_3 a H_0(\delta_3 a)}{2H_1(\delta_3 a)} = -o(\epsilon^0) \\ &T_n \to \frac{2\delta_1 a H_{n-1}(\delta_3 a)}{\sigma_1 \delta_3 a[-(1+\nu)H_n(\delta_3 a) + 2H_{n-2}(\delta_3 a)]} \cdot \frac{(\delta_1 a/2)^{n-2}}{(n-2)!} \\ &\quad \to \begin{cases} \dfrac{2H_1(\delta_3 a)(\delta_1 a/\sigma_1)}{\delta_3 a[2H_0(\delta_3 a) - (1+\nu)H_2(\delta_3 a)]} = o(\epsilon^{-1}) & n = 2 \\ o(\epsilon^{n-3}) & n > 2 \end{cases} \end{aligned}\right\} \tag{5.8b}$$

In (5.8b), we see that T_2, and hence $\bar{Q}_\theta$, approaches infinity as $p/p_0 \to 0$. This is caused by the vanishing denominator Q_0 in (5.1) at the zero frequency. Finite results are obtainable if the shear is normalized by the factor M_0/a with

$$\bar{Q}_\theta' = \left(\frac{aQ_\theta}{M_0}\right)_{r=a} = \frac{6\kappa^2(1-\nu)a^2}{(1-\sigma_1)h^2}\left(\frac{\sigma_1}{\delta_1 a}\right)\bar{Q}_\theta \tag{5.9}$$

The limiting values of normalized moment and shear are then obtained by substituting (5.8) into (5.2) and (5.9):

$$\left.\begin{aligned} &\bar{M}_\theta \to 1 + \nu - \frac{2(1-\nu^2)K_2(\mu)}{2K_0(\mu) + (1+\nu)K_2(\mu)}\cos 2\theta \\ &\bar{Q}_\theta' \to -\frac{2(1-\nu)\mu K_1(\mu)}{(1+\nu)K_2(\mu) + 2K_0(\mu)}\sin 2\theta \end{aligned}\right\} \tag{5.10}$$

where use has been made of (5.5) and

$$\mu = -i\delta_3 a \to (12)^{1/2}\kappa(a/h) \tag{5.11}$$

If κ^2 is assumed to be $\frac{10}{12}$, the foregoing results agree with the statical solution given by Reissner.[4] Since, if $\kappa^2 = \pi^2/12$, the δ_3 in (2.4) duplicates the three-dimensional theory of plates for a wide range of frequencies, including the static case $p = 0$,[9] the subsequent numerical calculation is based on $\kappa^2 = \pi^2/12$ except for that in the Appendix.

2. $0 < p/p_0 < 1$

In this frequency range, values for $\bar{M}_\theta$ and $\bar{Q}_\theta$ are computed from (5.2) by a digital computer. The results with the time factor restored have the form

$$(R + iI)e^{-ipt} = (R^2 + I^2)^{1/2}\, e^{-i(pt-\gamma)} \tag{5.12}$$

where R and I denote the real and imaginary parts, respectively, the motion of the plate being periodic in time. If the time in each period T is reckoned from the instant at which the moment M_x of undisturbed state is maximum at $\theta = \pm\pi/2$, the real part then yields the value of $\bar{M}_\theta$ or $\bar{Q}_\theta$ at $t = 0$, and the imaginary part gives the value at $t = T/4$. The absolute quantity $(R^2 + I^2)^{1/2}$ is the maximum value of $\bar{M}_\theta$ or $\bar{Q}_\theta$ at the boundary, and γ is the phase angle.

Real and absolute values of $\bar{M}_\theta$ and $\bar{Q}_\theta$ at $\theta = \pm\pi/2$ and $\pm 3\pi/4$, respectively, are shown in Figs. 3–6 for $\nu = 0.3$. The imaginary parts and phase angles can be computed from (5.12).

On Fig. 3, the points along the vertical axes are taken from the statical values given in the Appendix. The line of $a/h = 0$ is taken from the plane stress solution. In Ref. 5 it was shown that the dynamic stress concentration factor in plane

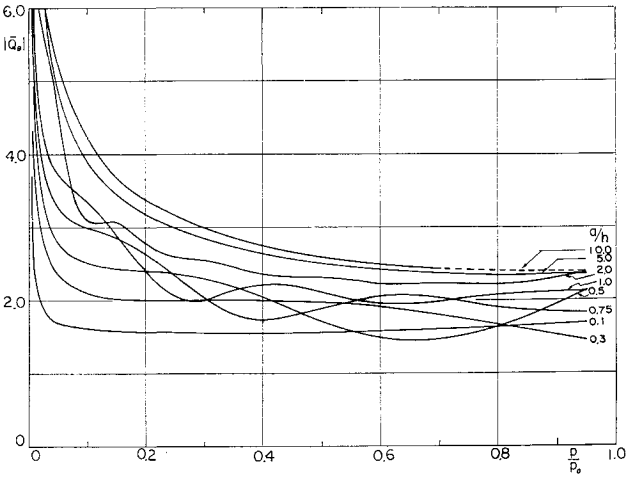

Fig. 4 Absolute values of normalized shear Q_θ at $r = a$, $\theta = 3\pi/4$ ($\nu = 0.30$).

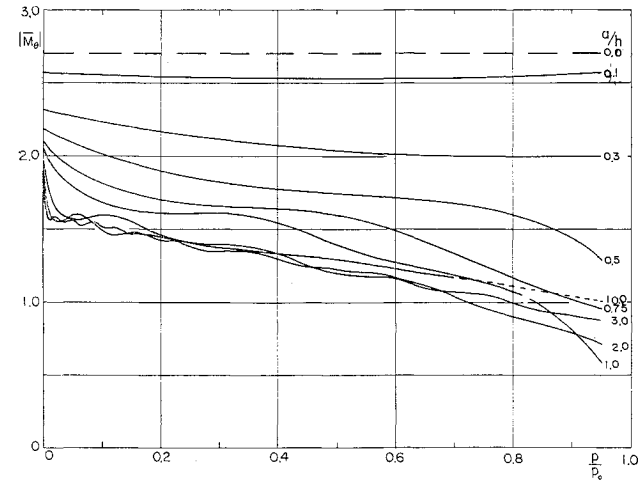

Fig. 5 Real values of normalized bending moment M_θ at $r = a$, $\theta = \pi/2$ ($\nu = 0.30$).

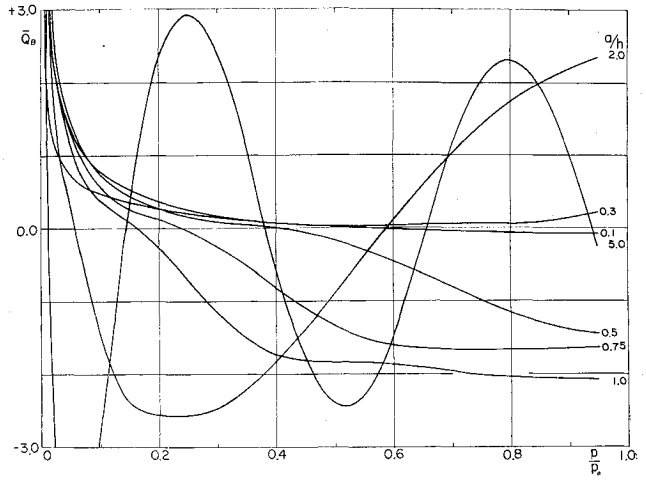

Fig. 6 Real values of normalized shear Q_θ at $r = a$, $\theta = 3\pi/4$ ($\nu = 0.30$).

stress changes with the frequencies. On this plot, $\bar{M}_\theta$ appears as a horizontal line because the reference frequency p_0 is infinite when $a/h = 0$.

For all other a/h ratios, and within the frequency range considered, the dynamical moment concentration factors are always less than the statical one. They decrease with increasing frequencies for a fixed a/h ratio and increase with decreasing a/h ratios at a constant frequency.

Instead of M_0/a, the shear Q_0 in the undisturbed state is used to normalize Q_θ. The reason is that Q_0 has a value different from zero except at $p = 0$, and Q_θ/Q_0 shows clearly the effect of a cavity on the stress distribution, whereas in the statical case, the shear is zero (see Appendix), and one is left with no choice.

The infinity of $\bar{Q}_\theta$ at $p/p_0 = 0$ (Figs. 4 and 6) is caused by the vanishing denominator Q_0 at zero frequency. When frequency increases, so does Q_0, and the shear concentration factors decrease steadily.

VI. Remarks

In the previous section, $\bar{M}_\theta$ and $\bar{Q}_\theta$ are calculated for $p < p_0$. For higher frequencies, the same Eqs. (5.2) and (5.3) can be used with all wave numbers being real. At $p = p_0$, a different set of equations remains to be derived.

In addition to the incident slow flexural waves considered here, two other types of incident waves, the fast flexural and thickness shear, may also be analyzed. But at low frequencies ($p < p_0$), both waves attenuate gradually from the source of loading, and they are of less interest than the slow flexural waves.

A steady-state flexural vibration of plate can be represented by

$$\eta_1^{(i)} = \eta_0 \cos\delta_1 x e^{-ipt} \qquad \eta_2^{(i)} = \eta_3^{(i)} = 0$$

They are just the real part of (3.1a) where the time factor is omitted. Thus, moment and shear concentrations around a cavity in a transversely vibrating plate are also given in this study. They are simply the real parts of (5.2), shown in Figs. 5 and 6.

Appendix

When a plate is in statical bending with

$$M_x = M_0 \qquad M_y = M_{xy} = Q_x = Q_y = 0 \qquad \text{(A1)}$$

at infinity, the bending moment and shear around a circular cavity in the plate are[4]

$$\frac{M_\theta}{M_0} = 1 - \frac{1}{2}\left[1 + \frac{3(1+\nu)K_2(\mu) - 2K_0(\mu)}{(1+\nu)K_2(\mu) + 2K_0(\mu)}\right]\cos 2\theta' \qquad \text{(A2)}$$

$$\frac{aQ_\theta}{M_0} = -\frac{2\mu K_1(\mu)}{(1+\nu)K_2(\mu) + 2K_0(\mu)}\sin 2\theta' \qquad \text{(A3)}$$

where $\mu = (10)^{1/2}\, a/h$, and θ' is an angle measured from x axis.

If a moment $M_y = \nu M_0$ is added to the plate, by principle of superposition,

$$\bar{M}_\theta = \left(\frac{M_\theta}{M_0}\right)_{\theta'=\theta} + \nu\left(\frac{M_\theta}{M_0}\right)_{\theta'=\theta-\pi/2} =$$

$$1 + \nu - \frac{2(1-\nu^2)K_2(\mu)}{(1+\nu)K_2(\mu) + 2K_0(\mu)}\cos 2\theta \qquad \text{(A4)}$$

Similarly,

$$\bar{Q}_\theta' = -\frac{2(1-\nu)\mu K_1(\mu)}{(1+\nu)K_2(\mu) + 2K_0(\mu)}\sin 2\theta \qquad \text{(A5)}$$

The maximum $\bar{M}_\theta$ and $\bar{Q}_\theta'$ occur at $\theta = \pm\pi/2$ and $\pm\pi/4$ (also $\pm 3\pi/4$), respectively. Values of maximum $\bar{M}_\theta$ and $\bar{Q}_\theta'$ are shown in Fig. 7 for various a/h and five values of Poisson's ratio.

If $\mu = \pi\, a/h$, which appears in the limiting case of dynamical solution with $\kappa^2 = \pi^2/12$, the values of $\bar{M}_\theta$ and $\bar{Q}_\theta'$ differ from those shown in Fig. 7 by less than 0.2%. The difference hardly can be shown on the graph.

Figure 7 shows that, as a/h increases, the $\bar{Q}_\theta'$ increases without bound. This, however, does not mean that the shear may become infinitely large in a thin plate with large cavity. Note that the normalization factor $M_0 \cong F(2h/3)$, where F, the average force acting on the upper or lower

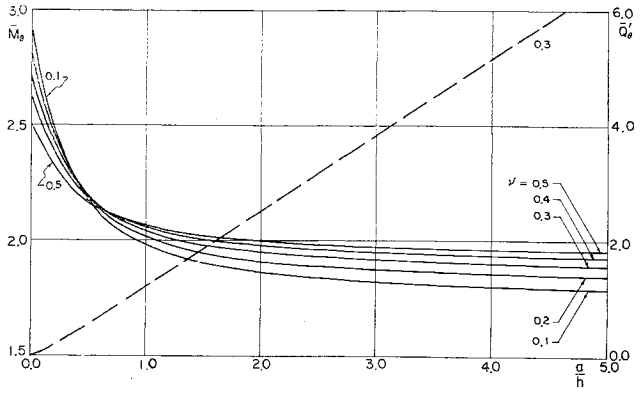

Fig. 7 Statical values of stress concentration factors for M_θ at $\theta = \pi/2$ (solid line) and Q_θ at $\theta = \pi/4$ (dash line).

half of the plate cross section, remains finite. Thus $\bar{Q}_\theta'$ has a built-in factor a/h from normalization. Since the right-hand side of (A5) and $\bar{Q}_\theta'$ ($\approx 3aQ/2hF$) approach infinity in the same order of a/h, the actual shear Q_θ remains finite.

References

[1] Mindlin, R. D., "Influence of rotatory inertia and shear on flexural motions of isotropic, elastic plates," J. Appl. Mech. **18**, 31 (1951).

[2] Kane, T. R., "Reflection of flexural waves at the edge of a plate," J. Appl. Mech. **21**, 213 (1954).

[3] Timoshenko, S. P. and Woinowsky-Krieger, S., *Theory of Plates and Shells* (McGraw-Hill Book Co., Inc., New York, 1959), p. 319.

[4] Reissner, E., "The effect of transverse shear deformation on the bending of elastic plates," J. Appl. Mech. **12**, A-69 (1945.)

[5] Pao, Y.-H., "Dynamical stress concentration in an elastic plate," J. Appl. Mech. **29**, 299 (1962).

[6] Chao, C. C. and Pao, Y.-H., "On the flexural motions of plates at cut-off frequency," J. Appl. Mech. **31**, 22 (1964).

[7] Mindlin, R. D. and Deresiewicz, H., "Thickness-shear and flexural vibrations of a circular disk," J. Appl. Phys. **25**, 1329 (1954).

[8] Morse, P. M. and Feshbach, H., *Methods of Theoretical Physics* (McGraw-Hill Book Co., Inc., New York, 1953), p. 1377.

[9] Mindlin, R. D., "An introduction to the mathematical theory of vibrations of elastic plates," U. S. Army Signal Corps Engineering Labs., Fort Monmouth, N. J., pp. 5–25 (1955).

[10] Rayleigh, J. W. S., *The Theory of Sound* (Dover Publications, Inc., New York, 1945), Vol. 1, p. 358.

[11] Onoe, M., *Tables of Modified Quotients of Bessel Functions* (Columbia University Press, New York, 1958).

[12] McLachlan, N. W., *Bessel Functions for Engineers* (Oxford University Press, London, 1955), p. 190.

NOVEMBER 1964 AIAA JOURNAL VOL. 2, NO. 11

Constants of the Motion for Optimum Thrust Trajectories in a Central Force Field

SAMUEL PINES*
Analytical Mechanics Associates, Inc., Uniondale, N. Y.

This paper derives four constants of the motion for optimal thrust trajectories in a central force field. Two additional constants of the motion are derived which hold for singular thrusting arcs as well as impulsive thrusts. The paper applies the constants of the motion for the impulsive thrust case to obtain a set of initial conditions for the classical adjoint variables to be used as a good approximation for a solution of the finite thrust arc by the indirect method.

Introduction

THE constants of the motion of a system of differential equations play an important role in characterizing the solutions. This paper develops an application of the constants of the motion to the indirect methods for obtaining solutions of optimal thrust trajectories by iterative procedures.

The optimal trajectories for a thrusting vehicle in a central force field have been under study for some time by Lawden,[1, 2] Leitmann,[3, 4] Melbourne,[5] Breakwell,[6] and others.† Four constants of the motion for this problem are well known. This paper derives two additional constants of the motion which hold for singular thrusting arcs and impulsive thrusts. The paper also derives the four known constants of the motion. The paper applies the constants of the motion for the impulsive thrust case to obtain a set of initial conditions for the classical adjoint variables to be used as a good approximation for the solution of the finite thrust arc by the indirect method.

As is well known, the indirect methods for obtaining solutions of the optimal thrust trajectories by iterative procedures suffer from an extreme sensitivity of the solution to small changes in the initial conditions of the adjoint variables. In effect, the success of the gradient techniques, employed by Kelley[7] and Bryson,[8] is largely due to their ability to control the incremental step size for small changes in the thrusting logic.

Once a good approximation to the optimum control thrust logic has been obtained, the gradient techniques prove too slow for convergence and resort is made to the classical indirect methods for the last few iterations. If a good approximation to the initial conditions of the adjoint variables were available, the indirect methods would be in more general use.

A good approximation to the initial conditions of the adjoint variables for a given problem may be obtained through a study of the limiting impulsive solution to the same problem. Let us assume that a solution to an optimal thrust trajectory exists and that it is known. Then, if one could improve the efficiency of the engine (thrust/weight ratio), a shorter burning arc could be obtained for an improved optimal trajectory. In the limit one would obtain the impulsive thrust solution of the given problem which would indeed require a perfect engine. Thus, we can look at the impulsive solution as a limiting point in a simply connected region in the space of the initial conditions of the adjoint variables. Intuitively, one might expect that an iterative procedure could be developed which would start with the known impulsive solution and converge to the required finite thrust solution.

This report applies the constants of the motion for an optimal impulsive trajectory to obtain approximate values

Presented at the Joint AIAA-IMS-SIAM-ONR Symposium on Control and System Optimization, Monterey, Calif., January 27–29, 1964 (not preprinted); revision received June 5, 1964. This study was performed under Contract NAS 8-5314 for the Future Projects Branch, Aeroballistics Division, of NASA Marshall Space Flight Center, Huntsville, Ala.

* President. Member AIAA.

† The author has been informed of a similar study by Hillsley and Robbins of IBM applying impulsive thrusts to optimum fuel trajectories for bounded thrust and fixed transfer time.